

Surface segregation driven by molecular architecture asymmetry in polymer blends

Jae Sik Lee, Nam-Heui Lee, Somesh Peri, and Mark D. Foster*
Department of Polymer Science, The University of Akron, Akron, Ohio 44325, USA

Charles F. Majkrzak
National Institute of Standards and Technology, Gaithersburg, Maryland 20899, USA

Renfeng Hu and David T. Wu
Department of Chemical Engineering and Department of Chemistry, Colorado School of Mines, Golden, Colorado 80401, USA
(Received 10 June 2014; revised manuscript received 27 October 2014; published 26 November 2014)

The contributions of chain ends and branch points to surface segregation of long-branched chains in blends with linear chains have been studied using neutron reflectometry and surface-enhanced Raman spectroscopy for a series of novel, well-defined polystyrenes. A linear response theory accounting for the number and type of branch points and chain ends is consistent with surface excesses and composition profile decay lengths, and allows the first determination of branch point potentials. Surface excess is determined primarily by chain ends with branch points playing a secondary role.

DOI: 10.1103/PhysRevLett.113.225702

PACS numbers: 64.75.Va, 64.75.St, 68.35.bm, 78.30.-j

Self-assembly is important for a wide range of applications, including the creation of functional nanostructures and segregation of species to surfaces to impart desirable properties to them. The structure resulting from self-assembly often depends on a balance of enthalpic and entropic forces. Conventionally, the preferential segregation of one polymer to the surface of a polymer blend is driven by the bulk tendency to demix, generally associated with differences in the repeat chemistry of the two polymers [1–7]. However, surface segregation can occur in a blend of polymers having the same repeat chemistry due only to differences in chain sizes [8–12] or molecular architecture [13–15]. Recent results reveal that differences in architecture can also strongly impact the dynamics at and near surfaces [16], polymer aging [17], and wetting [18]. Chain connectivity has been hypothesized to play a role in cooperative rearrangement important to dynamics near the glass transition [19], and so architecture-driven surface segregation can alter the surface glass transition. These dependences of properties upon molecular architecture open new avenues for the design of materials with unique properties.

Theory predicts that adding long chain branching to one component can lead to a preference of that species for the surface [13,20]. Self-consistent mean field theory simulations by Walton and Mayes [20] demonstrated that the near-surface concentration of branched polymers having a comblike structure increases with an increasing number of branches when these chains are mixed with a matrix of linear chains. These results are consistent with the predictions from a general linear response theory by Wu and Fredrickson for the effects of architectural asymmetry on binary blend surface thermodynamics [13]. While surface segregation involves entropic considerations including chain stretching and compositional variations [4,5,21,22],

the linear response theory suggests these complex contributions to the driving force for segregation can be simply understood in terms of effective surface potentials for the ends and branch points. Surface segregation due to branching was observed experimentally by Walton and co-workers [14] using neutron reflectivity (NR) of blends of linear poly (methyl methacrylate) (PMMA), and branched random copolymer of methyl methacrylate and methoxy poly(ethylene glycol) monomethacrylate [P(MMA-r-MnG)]. The P(MMA-r-MnG) species segregated to the air-polymer and substrate-polymer interfaces due to branching. Segregation driven by star branching has also been demonstrated experimentally by Greenberg *et al.* [15]. Archer and co-workers [23] did not directly measure surface segregation but measured how the surface energy of star-linear blend melts varied with the molecular architecture of the star-branched chains. They interpreted the variation in surface energy with blend composition using both a Cahn-Hilliard model and self-consistent field theory (SCFT). They concluded that the SCFT lattice simulations are only able to capture the substantially nonlinear variation in surface energy with composition by introducing an unrealistically large bulk thermodynamic interaction parameter, χ . In contrast, the Cahn-Hilliard model incorporating substantial empirical information on the pressure-volume-temperature behavior of the two components is more successful in rationalizing the observed dependences of surface energy on composition. Stein and collaborators [24] have very recently studied the interfacial segregation of bottlebrush copolymers having norbornene backbones and polystyrene arms in blends with linear chains.

The hypothesis regarding the roles of the chain ends and branch points mentioned above in connection with the linear response theory can be tested using neutron reflectometry

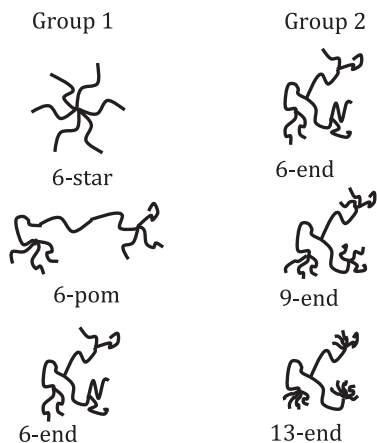


FIG. 1. Structures of the branched polystyrenes and abbreviated names. In group 1 the number of ends was fixed at 6 and the number of branch points varied from 1 to 4. In group 2 the number of ends varied from 6 to 13 and the number of branch points fixed at 4.

measurements with blends containing branched chains of well-defined architecture. Since branching generally leads to both an increase in the number of chain ends and to an increase in the number of branch points as well as changes in branch point chemistry, experimentally separating the contributions of these three features to the surface segregation is nontrivial. In particular, it requires the synthesis of well-defined branched polymers. In this Letter we report experimental measurements of surface segregation in architecturally asymmetric blends of long-branched and linear polystyrene (PS) chains that confirms that the simple consideration of surface potentials of chain ends and branch points separately, suggested by Wu and Fredrickson [13], captures the key features of the surface segregation.

Key to the study was the design and anionic synthesis of two groups of novel, well-defined, highly branched polystyrenes (Fig. 1, namely, *f*-star, *f*-pom, and *f*-end) [25], involving the use of a novel synthetic method. In group 1 the number of branch points in the molecule was varied from 1 to 3 to 4, while the number of ends was fixed at 6. In a second group the number of branch points was fixed

at 4 and the number of ends varied from 6 to 9 to 13. The molecular weights, numbers of end groups, and the numbers of branch points are listed in Table I for each branched polystyrene as well as for hydrogenous (L-hPS) and deuterated linear polystyrene (d-PS) analogs. The polydispersity for each polymer was below 1.05, and the overall molecular weight controlled to be ~ 36 kg/mol to exclude the possibility that interfacial segregation could be driven by molecular weight differences. The end group for all ends on branched chains was the butyl fragment from the butyllithium initiator used in the synthesis. The linear chain had one end with a butyl fragment and one end with a proton. Four types of junctions (described in Ref. [25]) are contained in the molecules. The star molecule contains disilylethylene, which is a flexible core. The pom-pom molecule has a difunctional initiator fragment (considered here as a branch point) at its center and the remainder of a silicon-based linking agent at each tetrafunctional junction. All the end-branched stars have a trifunctional initiator fragment at their centers, with fragments of silicon-based linking agents where the outer arms are connected to the three arms of the central star. The outer branch points in the 6-pom and the outer branch points in the 9-end are the same (from silicon tetrachloride). In each case where PS arms are linked to a Si-containing junction, one or two units of butadiene are present in the arm to facilitate linking. These units add to the flexibility of the junction. No butadiene units are present adjacent to the trifunctional initiator fragments (that are the central junction points). Each binary blend was prepared by dissolving amounts of PS and linear d-PS into toluene to make a blend with 20 vol. % PS. Silicon substrates were cleaned with a solution (7/3 by volume) of sulfuric acid and hydrogen peroxide [26] and etched with HF solution to remove the native oxide. Films of approximately 950 Å thickness were spun cast onto 7.7 cm diameter substrates. After drying in roughing vacuum, these films were annealed in high vacuum at 180°C for 12 h.

NR measurements performed on the NG-1 reflectometer at the National Institute of Standards and Technology revealed the concentration profiles of the branched PS normal to the air-polymer interface. The scattering length

TABLE I. Molecular characterization of polystyrenes.

Polymer	Arm M_n^a (g/mol)	Precursor M_n^a (g/mol)	Total M_n^a (g/mol)	α^b	ω^c
Linear	/	/	/	0	2
6-star	6300	/	36 300	1	5.8
6-pom	3800	18 200	40 500	3	5.8
6-branch	3000	18 100	35 800	4	5.9
9-branch	2400	17 700	38 900	4	9.0
13-branch	1300	17 700	34 200	4	13.0
d-PS	/	/	36 000	0	2

^aDetermined by GPC with three detectors: refractometer, viscometer, and light scattering.

^bNumber of branch points.

^cNumber of chain ends.

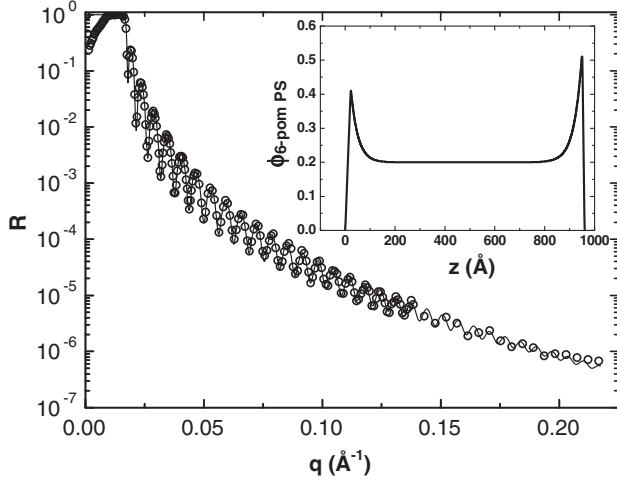


FIG. 2. Neutron reflectivity as a function of scattering wave vector, q , for a blend of 20 vol % 6-end PS with linear d-PS after annealing 12 h at 180 °C. The solid line represents the reflectivity calculated from the model concentration depth profile shown in the inset.

density (SLD) profiles of the films were obtained by minimizing the normalized sum of squared error (χ^2) between a reflectivity curve calculated from a parametrized model depth profile and the experimental reflectivity data. The shape expected from linear response theory [13] for the branched chain segment concentration profile is roughly an exponential decay with the addition of a small peak in the concentration slightly below the surface. A profile of approximately exponential shape proved sufficient to fit all the data shown here. With the resolution available it is not possible to either substantiate or deny the possibility of a small local maximum in branched chain segment concentration near the surface. The quantities in which we are primarily interested, the surface excess and the decay length, are not substantially impacted by this approximation. An example of the modeling for the blend with the 6-pom chain is shown in Fig. 2. The SLD profiles were converted to concentration depth profiles using the known SLDs of the two pure components. While the unannealed blend films showed no segregation at the surface and a very small interfacial excess at the substrate, all annealed blend films exhibited quantifiable segregation at both

interfaces. Here we focus on the surface excess, Γ , for each blend, listed in Table II, which was calculated as $\Gamma = \int_0^\infty [\phi(z) - \phi_\infty] dz$, where $\phi(z)$ is the volume fraction of the segregated component at a depth, z , for the annealed sample and ϕ_∞ is the bulk volume fraction. The driving force for surface segregation due to the isotopic difference between the two components alone is estimated using results for the linear-linear blend. The d-PS enriches the surface of the linear-linear blend modestly. In all five blends with architectural asymmetry, the branched component is enriched at the surface, even though the difference in isotopic labeling of the components favors d-PS at the air surface. The surface excess increases monotonically, but slowly with the number of branch points among the blends in which the number of chain ends was fixed at six (i.e. 6-star < 6-pom < 6-end).

Surface composition (as opposed to surface excess) was probed independently using surface enhanced Raman spectroscopy (SERS). Study by SERS requires that the surfaces be coated with metal droplets of the appropriate size. The coating was accomplished by first thermally evaporating, at $4\text{--}5 \times 10^{-7}$ Torr, a silver layer of 4.5 nm nominal thickness onto a previously annealed sample held at room temperature and then allowing the silver layer to dewet to form droplets. Samples of known surface composition were made for calibration of the SERS peak intensities using blend films that had not been annealed. In SERS spectra, the characteristic band due to the benzene ring breathing mode appears at 975 cm^{-1} for d-PS and at 1014 cm^{-1} for h-PS. [12] The ratio of the intensities of these two peaks corresponds to the weighted average composition of the h-PS integrated over the depth probed by the enhanced electric field about the droplets, using a depth-dependent field strength that drops off exponentially with a characteristic decay length [27] of ~ 2 nm. The spectra for the annealed films are presented in Fig. 3. The intensity of the peak corresponding to h-PS increases and the intensity of the peak for d-PS decreases as the architecture of the hydrogenous polymer changes from linear to 13-end. The near-surface compositions of h-PS inferred from the SERS measurements are compared in Table II with near-surface compositions deduced from the composition depth profiles from the NR data by averaging over the depth probed by SERS. Trends in surface

TABLE II. Characteristics of concentration profiles: Experiment compared with theory.

h -chain	σ (Å)	NR Surface Excess (Å)	NR concentration averaged over SERS sampling depth (± 0.02)	SERS surface concentration (± 0.03)	NR decay length (Å) (± 3 Å)	Theory decay length (Å)
L-hPS	4.9	-2 ± 0.5	0.16	0.16	10	
6-star	4.9	6 ± 1	0.30	0.27	26	33
6-pom	5.3	8 ± 1	0.33	0.32	28	30
6-end	4.9	11 ± 1.5	0.35	0.44	29	30
9-end	3.9	22 ± 1.5	0.49	0.50	35	31
13-end	3.0	38 ± 2	0.66	0.75	36	29

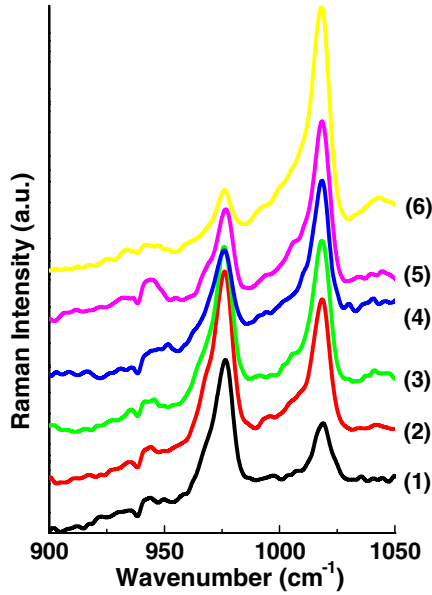


FIG. 3 (color online). SERS spectra for annealed blend films: (1) L-hPS/dPS blend, (2) 6-star/dPS, (3) 6-pom, (4) 6-branch/dPS, (5) 9-branch/dPS, and (6) 13-branch/dPS.

composition inferred from the two techniques are in good agreement.

Comparison is made to the linear response theory of Wu and Fredrickson [13] by solving for values of the surface potentials of the branch points and chain ends in each polymer that result in a best fit for the surface composition profile, subject to the constraint that the integrated surface excesses match the experimental values. The integrated surface excess is related by the theory to the surface potentials according to

$$\int_0^\infty dz \Delta \Phi(z) \approx \left(\frac{2}{N^L} U_e^L - \frac{n_j^B}{N^B} U_j^B - \frac{n_e^B}{N^B} U_e^B \right)$$

where N^B and N^L are the total numbers of monomers in the branched molecule (B) and linear molecule (L). U_i^J is the surface potential of the chain end ($i = e$) or junctions ($i = j$) for the branched ($J = B$) or the linear ($J = L$) molecule. n_j^B and n_e^B are the numbers of junctions and chain ends of the branched polymer, respectively.

We make simplifying assumptions on the basis of similarities in chemical functionality to close the system of equations. We assume that the difunctional branch point surface potential ($U_{j,2}^B$) and the central trifunctional branch

point surface potential ($U_{j,3}^B$) are the same because both branch point structures contain a phenyl ring and are more rigid than branch points that contain silicon and have butadiene units adjacent to the branch. It is necessary to distinguish the potentials of the two types of chain ends, butyl and proton. This is consistent with observations made in small angle neutron scattering studies of the bulk χ parameter for these blends. [28] There, the apparent enthalpic contributions to χ are proportional to the number of butyl end groups in the polymer.

With these assumptions we have relatively good fits of both the integrated excess and segregation depth (decay length) with the potentials listed in Table III, as shown in Table II. Our first conclusion is that attraction of the chain ends to the surface is substantially more important in driving the chains to the surface than is the attraction or repulsion of a branch point to the surface. A second inference is that the styrenelike chain end is attracted to the surface more strongly (by about a factor of 2) than is a chain end containing the butyl functionality. This is unexpected, since the cohesive energy density of a butyl material is less than that of PS. The magnitudes of the potentials for all three types of outer branch points are about a factor of 10 smaller than are the potentials of the end groups, and also at least a factor of four smaller than the magnitudes of the potentials of the inner branch points. So for these branch point and end group chemistries the surface segregation is driven primarily by end groups, with the branch points playing a secondary role. The branch point potentials are mostly negative in this case, and serve to enhance the surface segregation. The experimental and theoretical decay lengths are compared in Table II. The theoretical decay lengths at the air-polymer interface of all blends are approximately 30 Å, which is of the same magnitude as the experimental values.

Hariharan *et al.* [11] find using a lattice theory that in the neighborhood of the bulk upper critical solution temperature of a binary blend the strength of the surface segregation increases noticeably with the value of the segment-segment exchange interaction parameter, χ . Here we observe that the surface excess does vary generally with the bulk χ parameter [28]. Increasing the number of branch points with constant number of ends yields both modest changes in χ and in surface excess. χ increases markedly with the number of chain ends in this class of architectures and so does the surface excess. However, the

TABLE III. Surface potentials by fitting data to linear response theory. U_e^B , butyl end group; U_e^L , average of two end groups of a linear chain; $U_{j,2}^B$, joint at center of 6-pom (contains phenyl ring); $U_{j,3}^B$, inner joint of 6-end, 9-end and 13-end (trifunctional phenyl structure); $U_{j,3p}^B$, outer joint of 6-end (contains silicon); $U_{j,4}^B$, outer joint of 6-pom and 9-end (contains silicon); and $U_{j,6}^B$, joint at center of 6-star and outer joint of 13-end (contains silicon).

Surface Potential	U_e^B	U_e^L	$U_{j,2}^B$	$U_{j,3}^B$	$U_{j,3p}^B$	$U_{j,4}^B$	$U_{j,6}^B$
Value (ÅK)T	-26	-47	-16	-16	-2	-2	-4

mechanisms of segregation in the bulk and at the surface are, on the face of it, different. In the bulk, χ increases as differences in the bulk structure $S(k)$ factor increase, while the surface excess increases with the number and attractive strength of end and branch groups. This apparent difference in the mechanism can be reconciled by recognizing that the surface potentials for the ends are strongly attractive, and those of the branch points weak, and so greater branching leads to greater differences in $S(k)$ from a linear chain as well as greater total surface attraction.

In summary, the segregation at the air surface of blends containing well-defined polystyrenes of a variety of branched architectures has been quantified. The surface excess is determined primarily by chain ends with branch points playing a secondary role. A linear response theory that accounts for the number and type of branch points and chain ends, without regard for the way they are connected, is found to be consistent with these experimental results and also allows for the determination of the surface potential of branch points. Given the observation that branched chains have dramatically different surface fluctuations [16], these differences in surface segregation due to architecture could potentially be used to tailor dynamic as well as thermodynamic properties of polymer blend surfaces.

This research was supported by The American Chemical Society Petroleum Research Fund (No. 38915-AC7), NSF (CBET-0730692 and CBET-0731319), and by an Ohio Board of Regents challenge grant. Professor Roderic Quirk was instrumental in the design and synthesis of the molecules to enable the study and Professor Alexei Sokolov provided assistance with the SERS measurements and early discussions of the results.

*Corresponding author.
mfoster@uakron.edu

- [1] R. A. L. Jones, E. J. Kramer, M. H. Rafailovich, J. Sokolov, and S. A. Schwarz, *Phys. Rev. Lett.* **62**, 280 (1989).
- [2] R. J. Composto, R. S. Stein, E. J. Kramer, R. A. L. Jones, A. Mansour, A. Karim, and G. P. Felcher, *Physica B (Amsterdam)* **157**, 434 (1989).
- [3] R. A. L. Jones, L. J. Norton, E. J. Kramer, R. J. Composto, R. S. Stein, T. P. Russell, A. Mansour, A. Karim, G. P. Felcher, M. H. Rafailovich, J. Sokolov, X. Zhao, and S. A. Schwarz, *Europhys. Lett.* **12**, 41 (1990).
- [4] A. Hariharan, S. K. Kumar, M. H. Rafailovich, J. Sokolov, X. Zheng, D. Duong, S. A. Schwarz, and T. P. Russell, *J. Chem. Phys.* **99**, 656 (1993).
- [5] J. Genzer, A. Faldi, and R. J. Composto, *Phys. Rev. E* **50**, 2373 (1994).
- [6] J. Genzer, A. Faldi, R. Oslanec, and R. J. Composto, *Macromolecules* **29**, 5438 (1996).
- [7] J. Genzer and R. J. Composto, *Europhys. Lett.* **38**, 171 (1997).
- [8] A. Hariharan, S. K. Kumar, and T. P. Russell, *Macromolecules* **23**, 3584 (1990).
- [9] A. Budkowski, U. Steiner, and J. Klein, *J. Chem. Phys.* **97**, 5229 (1992).
- [10] P. Cifra, F. E. Karasz, and W. J. MacKnight, *Macromolecules* **25**, 4895 (1992).
- [11] A. Hariharan, S. K. Kumar, and T. P. Russell, *J. Chem. Phys.* **98**, 4163 (1993).
- [12] P. P. Hong, F. J. Boerio, and S. D. Smith, *Macromolecules* **27**, 596 (1994).
- [13] D. T. Wu and G. H. Fredrickson, *Macromolecules* **29**, 7919 (1996).
- [14] D. G. Walton, P. P. Soo, A. M. Mayes, S. J. Sofia Allgor, J. T. Fujii, L. G. Griffith, J. F. Ankner, H. Kaiser, J. Johansson, G. D. Smith, J. G. Barker, and S. K. Satija, *Macromolecules*, **30**, 6947 (1997).
- [15] M. D. Foster, C. C. Greenberg, D. M. Teale, C. M. Turner, S. Corona-Galvan, E. Cloutet, P. D. Butler, B. Hammouda, and R. P. Quirk, *Macromol. Symp.* **149**, 263 (2000).
- [16] S. F. Wang, S. Yang, J. Lee, B. Akgun, D. T. Wu, and M. D. Foster, *Phys. Rev. Lett.* **111**, 068303 (2013).
- [17] E. Glynos, B. Frieberg, H. Oh, M. Liu, D. W. Gidley, and P. F. Green, *Phys. Rev. Lett.* **106**, 128301 (2011).
- [18] E. Glynos, B. Frieberg, and P. F. Green, *Phys. Rev. Lett.* **107**, 118303 (2011).
- [19] P. G. de Gennes, *Eur. Phys. J. E* **2**, 201 (2000).
- [20] D. G. Walton and A. M. Mayes, *Phys. Rev. E* **54**, 2811 (1996).
- [21] L. J. Norton, E. J. Kramer, F. S. Bates, M. D. Gehlsen, R. A. L. Jones, A. Karim, G. P. Felcher, and R. Kleb, *Macromolecules* **28**, 8621 (1995).
- [22] I. Schmidt and K. Binder, *J. Phys. (Les Ulis, Fr.)* **46**, 1631 (1985); J. P. Donley and G. H. Fredrickson, *J. Polym. Sci. B* **33**, 1343 (1995); A. Yethiraj, *Phys. Rev. Lett.* **74**, 2018 (1995); D. T. Wu, G. H. Fredrickson, and J. P. Carton, *J. Chem. Phys.* **104**, 6387 (1996).
- [23] Z. Y. Qiang, V. S. Minnikanti, B. B. Sauer, G. T. Dee, W. G. Kampert, and L. A. Archer, *J. Polym. Sci. B* **47**, 1666 (2009).
- [24] I. Mitra, X. Li, S. L. Pesek, B. Makarenko, B. S. Lokitz, D. Uhrig, J. F. Ankner, R. Verduzco, and G. E. Stein, *Macromolecules* **47**, 5269 (2014).
- [25] J. S. Lee, R. P. Quirk, and M. D. Foster, *Macromolecules* **38**, 5381 (2005).
- [26] Piranha solution must be handled with care. Proper protective gear must be worn.
- [27] C. A. Murray and D. L. Allara, *J. Chem. Phys.* **76**, 1290 (1982).
- [28] J. S. Lee, M. D. Foster, and D. T. Wu, *Macromolecules* **39**, 5113 (2006).